BIOCHEMISTRY
including biophysical chemistry & molecular biology
Article

Biochemistry **2009,** *48,* 6811–6823 6811
DOI: 10.1021/bi9000276

A Fluorescent Mutant of the NM Domain of the Yeast Prion Sup35 Provides Insight into Fibril Formation and Stability†

Fernando L. Palhano,‡ Cristiane B. Rocha,‡ Alexandre Bernardino,§ Gilberto Weissmuller,§ Claudio A. Masuda,‡ Mônica Montero-Lomelí,‡ André Marco Gomes,‡ Peter Chien,∥ Patrícia M. B. Fernandes,⊥ and Debora Foguel*,‡

‡*Instituto de Bioquímica Médica, Programa de Biologia Estrutural e Programa de Biologia Molecular e Biotecnologia and* §*Instituto de Biofísica Carlos Chagas Filho, Universidade Federal do Rio de Janeiro, Rio de Janeiro 21941-590, Brazil,* ∥*Department of Biology, Massachusetts Institute of Technology, Cambridge, Massachusetts 02139, and* ⊥*Núcleo de Biotecnologia, Universidade Federal do Espírito Santo, Vitória ES 29040-090, Brazil*

Received January 8, 2009; Revised Manuscript Received June 15, 2009

ABSTRACT: The Sup35 protein of *Saccharomyces cerevisiae* forms a prion that generates the [*PSI*$^+$] phenotype. Its NM region governs prion status, forming self-seeding amyloid fibers *in vivo* and *in vitro*. A tryptophan mutant of Sup35 (NM^{F117W}) was used to probe its aggregation. Four indicators of aggregation, Trp 117 maximum emission, Trp polarization, thio-T binding, and light scattering increase, revealed faster aggregation at 4 °C than at 25 °C, and all indicators changed in a concerted fashion at the former temperature. Curiously, at 25 °C the changes were not synchronized; the first two indicators, which reflect nucleation, changed more quickly than the last two, which reflect fibril formation. These results suggest that nucleation is insensitive to temperature, whereas fibril extension is temperature dependent. As expected, aggregation is accelerated when a small fraction (5%) of the nuclei produced at 4 or 25 °C are added to a suspension containing the soluble NM domain, although these nuclei do not seem to propagate any structural information to the growing fibrils. Fibrils grown at 4 °C were less stable in GdmCl than those grown at higher temperature. However, they were both resistant to high pressure; in fact, both sets of fibrils responded to high pressure by adopting an altered conformation with a higher capacity for thio-T binding. From these data, we calculated the change in volume and free energy associated with this conformational change. AFM revealed that the fibrils grown at 4 °C were statistically smaller than those grown at 25 °C. In conclusion, the introduction of Trp 117 allowed us to more carefully dissect the effects of temperature on the aggregation of the Sup35 NM domain.

Protein misfolding and aggregation have been implicated in several human and animal diseases, such as Alzheimer's, Parkinson's, and prion diseases (*1*). Among them, prion disease is the only one that is transmissible; the aggregates are infectious units that are able to recruit the soluble, cellular proteins of the host organism (*2*). This phenomenon was discovered during the study of the transmissible spongiform encephalopathies of mammals (*2*) but was later also found to occur in fungi with certain epigenetically inherited traits (*3*). *Saccharomyces cerevisiae* encodes at least seven different proteins, Sup35, Ure2, Rnq1, Swi1, Mca1, Cyc8, and Mot3, that can form transmissible aggregates that cause a non-Mendelian pattern of inherence during mating and division (*4*−*8*).

The *S. cerevisiae* prion [*PSI*$^+$] causes translational read-through of stop codons and is detected by the suppression of nonsense mutations (*9*). The [*PSI*$^+$] state is caused by self-propagating aggregates of the Sup35 protein, which is an essential translation termination factor (*4*). As a consequence, [*PSI*$^+$] cells that contain *ade1*−*14*, a nonsense mutation in *ADE1*, are able to grow in media lacking adenine because of sufficient read-through of *ade1*−*14*. In contrast, isogenic [*psi*$^-$] cells require adenine supplementation and have a red color due to the accumulation of a pigmented intermediate in adenine metabolism (*10*).

The Sup35 protein has three distinct regions: a glutamine/asparagine-rich N-terminal domain (N, amino acids 1−124) that has five imperfect nine-residue repeats and is necessary and sufficient for [*PSI*$^+$] formation, a highly charged middle region (M, amino acids 125−253), and a C-terminal domain (C, amino acids 254−686) that carries the translation termination function (*11*). The N and M regions, known collectively as the NM domain, govern prion status.

During the past few years, the NM domain of Sup35 has been widely studied in order to understand its role in prion biology and for its use as a model for prion diseases because it shares sequence

†This work was supported by grants from Conselho Nacional de Desenvolvimento Científico e Tecnológico (CNPq), Fundação Carlos Chagas Filho de Amparo à Pesquisa do Estado do Rio de Janeiro (FAPERJ), Millennium Institute for Structural Biology in Biomedicine and Biotechnology (CNPq Millennium Program), and Coordenação de Aperfeiçoamento de Pessoal de Nível Superior (CAPES) to D.F.

*Correspondence should be addressed to this author. E-mail: foguel@bioqmed.ufrj.br. Phone: (55-21) 2562-6761. Fax: (55-21) 2270-8647.

Published on Web 06/17/2009

similarity with the prion protein and a similar mechanism of transmissibility (*12*). *In vitro*, the NM domain forms self-seeding amyloid fibers (*11*, *13*). *De novo* NM polymerization is characterized by a long lag phase during which part of the protein oligomerizes to form a nucleus, followed by a cooperative assembly phase in which soluble proteins rapidly associate with the nucleus and convert to amyloid fibrils (*14*). The lag phase can be eliminated with the addition of preformed NM fibers or seeds (*14*, *15*).

Recently, studies performed by Lindquist's group have shown that during the initial steps of NM fiber formation the core of the fibril collapses into a nonamyloid solvent-protected state that is thought to facilitate intermolecular head-to-head interactions. The molecule then enters the amyloid state as fibers grow by head-to-head and tail-to-tail additions to form a β-helical structure (*16*). Contrary to this model, the crystal structure of a heptapeptide derived from Sup35 revealed an in-register parallel β-sheet organization in the amyloid fibril (*17*); this structure has been recently reinforced with solid-state NMR studies on the NM domain (*18*, *19*).

Introduction of pure Sup35 fibrils into yeast cells causes a conversion to [*PSI*$^+$] with varying prion phenotypes (*20*, *21*). When NM fibrils formed at 4 °C are introduced into [*psi*−] cells, a strong [*PSI*$^+$] phenotype is observed. However, when NM fibrils formed at 25 °C are introduced, they produce weak [*PSI*$^+$] strains (*21*). In light of this result, it is thought that the NM domain is capable of producing distinct amyloid conformations that are dependent upon the temperature at which the fibrils are grown. The distinct conformations have unique phenotypic consequences; i.e., fibrils produced at 4 °C are more fragile than those grown at 25 °C; this fragility can result in additional termini, which may allow for more efficient capture of soluble host proteins, a potential cause of the stronger phenotype observed *in vivo* (*22*).

Tryptophan (Trp)[1] fluorescence has been used successfully to study protein folding, association, and aggregation due to the high sensitivity of Trp emission to its local environment (*23*−*27*). Here, we have constructed a Sup35 mutant in which the Phe at position 117 of the NM domain is replaced by Trp (NM^{F117W}). NM has no endogenous Trp residues; position 117 was chosen because it lies in the transition zone between the N and M regions, a stretch that has been implicated in Sup35 fibril polymorphism (*15*). We show that this mutation does not compromise the physical properties of the NM domain, allowing us to use NM^{F117W} for further studies. Aggregation was slower at 25 °C than at 4 °C, and all four indicators of aggregation, viz., shift in Trp 117 maximum emission, Trp polarization, thioflavin T (thio-T) binding, and an increase in light scattering (LS), changed in a concerted fashion at the latter temperature. Curiously, the changes in these four indicators did not occur at similar times at 25 °C, but rather the first two indicators changed more quickly than the last two. These data show that the spectroscopic changes associated with Trp emission, which seem to reflect nucleus formation, are temperature independent and display similar kinetics at 4 and 25 °C. However, thio-T binding and the increase in LS, which reflect fibril formation, were sensitive to the temperature at which fibrils were grown; the indicators occurred more quickly at 4 °C. We also investigated the stability of fibrils grown at both temperatures against GdmCl and demonstrated that fibrils produced at 4 °C were less stable than fibrils grown at 25 °C. Both fibrils were resistant to high pressure as they assumed an altered conformation that binds thio-T with a greater capacity. AFM measurements revealed that the fibrils grown at 4 °C were statistically smaller than those grown at 25 °C.

[1]Abbreviations: AFM, atomic force microscopy; CD, circular dichroism; FCS, fluorescence correlation spectroscopy; FITC, fluorescein isothiocyanate; GdmCl, guanidinium chloride; HHP, high hydrostatic pressure; LS, light scattering; Phe, phenylalanine; thio-T, thioflavin T; Trp, tryptophan; YPD, yeast peptone and dextrose medium.

EXPERIMENTAL PROCEDURES

Materials. Oligonucleotides were obtained from DNAgency; Taq polymerase, T4 DNA ligase, and restriction endonucleases were acquired from Invitrogen. Acrylamide and thio-T were obtained from Sigma. All other reagents were of analytical grade.

Plasmid Construction. DNA manipulations were carried out according to standard procedures (*28*). Genomic DNA of strain W303-1A (MATa *ade2 his3 leu2 trp1 ura3*) was used as a template to amplify wild-type (wt) Sup35NM by PCR with the following primers: forward 5′-C GCG GAT CCG ATG TCG GAT TCA AAC CAA GG-3′ and reverse 5′-AGG GAG CTC ACC ACC AAA CAT ATC GTT AAC-3′. The PCR was conducted with 30 cycles of heat denaturation at 94 °C for 1 min, primer annealing at 53 °C for 1 min, and DNA chain extension at 72 °C for 3 min, and a final extension at 72 °C for 10 min. The PCR products were resolved through 1% agarose and isolated using a QIAquick gel extraction kit (Qiagen). The DNA from Sup35NM wt was digested with *Bam*HI and *Sac*I and cloned into pBlueScript II for sequencing. Sup35NM was amplified from pBlueScript II using primers that introduce a His tag at the C-terminus (*29*). This product was subcloned into *Nde*I/*Eco*RI sites of the T7 expression plasmid pAEd4. The natural occurrence of a unique *Eco*RV restriction site near the target position allowed us to create a new forward primer 5′-G CAA GGA TAT CAA GCT GGT **TGG** CAA CCA CAG-3′ that harbors the F117W mutation (bold) and *Eco*RV site. The DNA fragment containing the F117W mutation was then created by PCR using the above forward primer and the aforementioned reverse primer that was used for Sup35NM wt construction. This fragment was cloned into *Eco*RV/ *Sac*I sites of Sup35NM wt pBlueScript II to create Sup35NM F117W pBlueScript II. Construction of the mutated pAEd4 plasmid was carried out as described for Sup35NM wt (*29*).

Gene Integration and Replacement. Yeast strains expressing *SUP35* with the F117W domain were generated by replacing the wild-type chromosomal locus in the parental strain 74-D694 [*PSI*$^+$] (MATα *ade1*−*14 his3 leu2 trp1 ura3*), as described previously (*29*, *30*). The gene was introduced by treating the cells with lithium acetate (*31*).

Protein Expression and Purification. Pure NM^{wt} and NM^{F117W} were prepared as described previously (*32*). Briefly, cells were lysed by sonication in buffer A (20 mM Tris-HCl, 8 M urea, pH 8.0). The lysate was cleared of debris by centrifugation at 30000*g* for 20 min at 10 °C. The supernatant was passed through an affinity column with Ni^{2+} (chelating Sepharose; Amersham) preequilibrated with buffer A. The column was washed with 5 column volumes of buffer B (20 mM Tris-HCl, 8 M urea, 40 mM imidazole, pH 8.0) and eluted with buffer C (20 mM Tris-HCl, 8 M urea, 400 mM imidazole, pH 8.0). Pooled fractions were applied to a Q-Sepharose Fast Flow column (Pharmacia) preequilibrated with buffer C. The column was washed with 5 bed volumes of 20 mM Tris-HCl, 8 M urea, and 100 mM NaCl, pH 8.0, and eluted with 300 mM NaCl in the same

buffer. The pure protein was concentrated with a Centricon 5 kDa (Millipore) and filtered with a Centricon 100 kDa (Millipore). Protein concentration was determined by UV absorption at 280 nm, using an extinction coefficient (ε) of 29800 M^{-1} and 35300 M^{-1} for wt and F117W, respectively.

Aggregation of Sup35NM. A concentrated NM solution was diluted at least 200-fold into phosphate buffer (5 mM potassium phosphate, 150 mM NaCl, pH 7.4) to a concentration of 5 μM. Reactions were carried out at 4 or 25 °C under constant gentle agitation (60 rpm) with a microstir bar. In the experiments where nuclei were used to nucleate a fresh, soluble sample of NM^{wt}, samples were incubated for the indicated times (20 min) under aggregating conditions, after which 5% (w/w) of this solution was transferred to a fresh solution of NM^{wt} (4.75 μM). Aggregation was continued in the absence of agitation, either at 4 or 25 °C, and was monitored by the Congo Red (CR) spectral shift assay as reported previously (*32*).

Limited Proteolysis of Sup35NM Fibrils. Fibrils were produced under agitation for 4 h at 4 or 25 °C and then centrifuged at 20000*g* for 1 h at 10 °C. Pellets were resuspended in phosphate buffer and incubated with chymotrypsin (1/250, w/w) for 15 min at 25 °C (*21*). The reaction was stopped by the addition of SDS, and the solution was boiled for 10 min. The samples were separated via 12% SDS−PAGE and stained with Coomassie Brilliant Blue R-250.

Characterization of NM Assembly by SDS Solubility. The nonfibrillar NM domain remains soluble in 2% (w/v) SDS while the amyloid fibrils are insoluble in SDS at room temperature (*32*). Soluble NM (5 μM) was stirred (60 rpm) at 25 or 4 °C while aliquots (20 μL) were withdrawn at various time intervals. The aliquots were incubated in the presence of 2% SDS at room temperature prior to being subjected to 12% SDS−PAGE. As a control, fibrils grown at 4 or 25 °C for 150 min were produced, boiled for 10 min in the presence of 2% SDS, and resolved by electrophoresis. The gels were stained with Coomassie Blue. The bands were quantified by Image J (http://rsb.info.nih.gov/ij/). Error bars represent the SD of two measurements.

Spectroscopic Measurements. All spectroscopic measurements were performed in an ISS spectrofluorometer (Champaign, IL) using a slit width of 1 nm for excitation and emission. Scattered light (320 nm) was measured at an angle of 90° from the incident light and quantified by integrating the intensity at 315−325 nm. A wavelength of 450 nm was used to excite thioflavin T (20 μM) while emitted fluorescence was recorded from 460 to 520 nm.

Tryptophan emission was performed by exciting the samples at 295 nm (the fluorescence contribution of tyrosine residues is minimized at this wavelength) and collecting the emission from 315 to 400 nm. The average energy of the fluorescence emission spectra was calculated as the center of spectral mass $\langle \nu \rangle$:

$$\langle \nu \rangle = \sum\nolimits_{\nu_i} F_i / \sum F_i \qquad (1)$$

where F_i is the fluorescence emitted at wavelength ν_i. The extent of reaction (α) is related to $\langle \nu_t \rangle$ by the expression

$$\alpha = (\langle \nu_t \rangle - \langle \nu_i \rangle)/(\langle \nu_i \rangle - \langle \nu_f \rangle) \qquad (2)$$

where $\langle \nu_i \rangle$ and $\langle \nu_f \rangle$ are the initial and final values of the center of spectral mass in nanometers, respectively, while $\langle \nu_t \rangle$ is the center of spectral mass at time *t*.

Fluorescence Polarization. Fluorescence polarization was measured in an ISS-PC1 spectrofluorometer (ISS, Champaign, IL) and calculated from $p = (I_{\parallel} - I_{\perp})/(I_{\parallel} + I_{\perp})$, where $I_{\parallel}$ and $I_{\perp}$ are the intensities of the emission when the polarizers were oriented parallel or perpendicular, respectively, to the polarizer of the exciting light. The samples were excited at 295 nm and filters WG335 and 7-54 were used in the emission.

Acrylamide Quenching. Tryptophan fluorescence quenching experiments were performed with NM^{F117W} (5 μM) in the soluble and aggregated states (4 or 25 °C). Aliquots of a stock solution of 9 M acrylamide were added to the samples, which were diluted in 5 mM potassium phosphate and 150 mM NaCl, pH 7.4. Excitation was set at 295 nm and emission collected from 315 to 400 nm. The spectra were corrected for blank and dilution effects. The data were analyzed according to the Stern−Volmer equation for collision quenching, $F_0/F = 1 + K_{SV}[Q]$, where F_0 and F are the initial steady-state emission intensities at λ_{max} in the absence and presence of acrylamide, respectively, [Q] is the molar concentration of acrylamide, and K_{SV} is the Stern−Volmer quenching constant (*24*).

Denaturation of Fibrils by GdmCl. Preformed fibrils at 4 or 25 °C were centrifuged at 20000*g* for 1 h at 10 °C and resuspended in phosphate buffer with increasing concentrations of guanidinium chloride (GdmCl). These suspensions were incubated at 25 °C for 2 h and then evaluated for thio-T binding and Trp emission.

Circular Dichroism. Circular dichroism (CD) measurements were performed in a Jasco-715 spectropolarimeter (Jasco Corp., Tokyo, Japan) using a 1.0 mm path-length quartz cuvette in 5 mM potassium phosphate and 150 mM NaCl, pH 7.4. NM^{wt} at 5 μM was gently agitated (60 rpm) with a microstir bar at 4 or 25 °C for 0, 15, 20, 25 min, and 4 h, after which their CD spectra were recorded. Wavelength scans were fixed with a 1 nm bandwidth and 0.4 s response time at 100 nm min^{-1} for five accumulations. The baselines (buffer alone) were subtracted.

High-Pressure Measurements. The high-pressure cell (*33*) was purchased from ISS (Champaign, IL). Fibrils at 5 μM grown at 4 or 25 °C were diluted in 20 mM Tris-HCl and 150 mM NaCl, pH 7.4, and subjected to increasing pressures at 25 °C in steps of 340 bar. Tris-HCl buffer was chosen because its pK_a does not change significantly under high pressure (*34*). At each pressure step the sample was allowed to equilibrate for 10 min prior to taking measurements. No time-dependent changes in fluorescence spectra were observed between 10 and 60 min. Fluorescence emission of free thio-T is not influenced by high pressure.

Thermodynamic Parameters. The standard volume change associated with fibril structure perturbation induced by HHP ($\Delta V_{F1 \rightarrow F2}$) and the equilibrium constant ($K_{F1 \rightarrow F2}$) associated with this process were determined from the thermodynamic relationship:

$$\ln[\alpha_p/(1-\alpha_p)] = p(\Delta V_{F1 \rightarrow F2}/RT) + \ln K_{F1 \rightarrow F2} \qquad (3)$$

where α is the extent of reaction, R is the gas constant, and T the temperature in kelvin at which the experiment was performed.

Atomic Force Microscopy Images. The fibrils or oligomers were diluted to 1 μM in phosphate buffer and placed directly onto freshly cleaved mica for 10 min in a volume of 50 μL. The samples were washed five times with 200 μL of ultrapure water and air-dried overnight. Tapping-mode AFM in air was performed using an Asylum MFP-3D BIO AFM (Asylum Research, Santa Barbara, CA) and Olympus rectangular silicon cantilevers with a resonance frequency of 70 kHz and nominal spring constant of 2 N/m. Samples were imaged at scan rates of

Table 1: Comparison of the $t_{1/2}$ (min) Values for the Changes Observed during Aggregation of Sup35 NM^{wt} or NM^{F117W} at 4 or 25 °C[a]

sample (T, °C)	thioflavin T	light scattering	center of spectral mass	polarization
wt (4)	40 ± 2 (11.37 ± 0.42)	37 ± 4 (10.12 ± 0.51)	ND	ND
wt (25)	67 ± 3 (15.27 ± 0.44)	60 ± 4 (17.42 ± 0.62)	ND	ND
F117W (4)	40 ± 3 (12.49 ± 0.53)	36 ± 5 (9.06 ± 0.41)	27 ± 3	27 ± 2
F117W (25)	67 ± 3 (20.66 ± 0.73)	58 ± 4 (18.08 ± 0.48)	24 ± 2	22 ± 3

[a] The slope of each curve is presented in parentheses. Data are means ± standard deviation of the mean of at least three independent experiments. ND = not determined.

0.5−1.0 Hz, and 512 × 512 pixels were collected per image. At least three regions of each surface were investigated to confirm homogeneity of the samples. Height measurements were estimated by section analyses using IGOR PRO (Wavemetrics, OR) with at least 150 individual fibrils from scan sizes of 2−5 μm. To measure the topological height of the fiber, 25 μm^2 of three independent images was analyzed using a threshold of 3 nm. For each image, the program analyzed ~22000 points. Each point corresponds to a touch of the tip to the surface of the fibril.

Sample Labeling and Fluorescence Correlation Spectroscopy (FCS) Measurements. Soluble NM^{wt} at 1 mM was incubated with 4 mM FITC in phosphate buffer (5 mM potassium phosphate, 150 mM NaCl, 6 M GdmCl, pH 7.4) for 90 min at 4 °C. The free probe was removed by extensive washing in a Centricon filter tube (10 kDa cutoff) (Millipore) at 25 °C. The labeled protein was filtered through a 100 kDa Centricon filter tube. The labeling efficiency was estimated by measuring the absorption at 494 nm ($\varepsilon = 68000\ M^{-1}$) and 280 nm ($\varepsilon = 29800\ M^{-1}$). The extent of labeling was estimated to be 40%, suggesting that the N-terminus is preferentially labeled at pH 7.4, as expected. Labeled nuclei were produced by incubating 5 μM FITC-labeled NM under gentle stirring at 25 °C for 20 min in Tris buffer (20 mM Tris-HCl, 150 mM NaCl, pH 7.4). The sample was then centrifuged at 20000*g* for 15 min at 15 °C to remove any fibril present. Five percent of these labeled nuclei (w/w) was then transferred to a solution of soluble NM (4.75 μM) to produce fibrils at 25 °C. FCS measurements were carried out in an ALBA fluorescence correlation spectrometer (ISS, Champaign, IL) using a Nikon TE2000-U inverted microscope with a two-photon excitation regime. A Ti:Sa Tsunami laser, pumped by a Millenia Pro 15sJ (Spectra Physics, Mountain View, CA), was focused on the sample with a water immersion 63× objective, 1.2 NA. A wavelength of 780 nm was used for FITC-labeled NM excitation. Fluorescence was collected through the same lens and separated from excitation by a dichroic mirror 700dcxru (Chroma, VT). After passing though the dichroic mirror, the beam was split by a 50/50 beam splitter, and the resulting beams were focused to two APD detectors. Recorded fluctuation traces were processed in Vista ISS software for autocorrelation and fitting calculations. Autocorrelation curves were fitted to a model function describing the free diffusion through a 3D Gaussian excitation volume obtained by two-photon excitation. From the curves fittings, the diffusion times τ_D were obtained and diffusion coefficients calculated from the relation $\tau_D = \omega_o^2/8D$ (*35*, *36*).

Data Processing. Each experiment was performed at least in triplicate, and the bars indicate the standard deviation of each point. The data in Figure 6 were evaluated statistically with an analysis of variance (ANOVA, Tukey's multiple comparison test) (*37*) using the software Prism (Graphpad Software, Inc., San Diego, CA).

RESULTS

Fibrillation Properties of NM^{F117W} in Vivo and in Vitro. The replacement of a phenylalanine (Phe) with a tryptophan (Trp) at position 117 does not alter the properties of the NM domain of Sup35 protein *in vitro* (Supporting Information, Figure S1). The replacement of a genomic copy of the gene encoding Sup35 in the yeast *S. cerevisiae* with one encoding $Sup35^{F117W}$ in a [*PSI*$^+$] strain does not abolish the [*PSI*$^+$] trait, as indicated by the white color of the cells plated on YPD medium (Supporting Information, Figure S1A). *In vitro* experiments show that NM^{F117W} forms fibrils at 4 and 25 °C at the same corresponding rates as wild-type protein when evaluated by thio-T binding (Supporting Information, Figure S1B); the $t_{1/2}$ values (time required to achieve 50% of aggregation) for NM^{F117W} were 40 ± 3 and 67 ± 3 min at 4 and 25 °C, respectively (Table 1).

It has been shown that fibrils grown at 4 °C are more susceptible to proteolysis than those grown at 25 °C; this finding suggests that there are differences in the packing and architecture of fibrils grown at different temperatures (*21*). Again, the digestion pattern of fibrils composed of NM^{F117W} was identical to that observed for wild-type fibrils (Supporting Information, Figure S1C,D). Furthermore, we probed the ability of NM^{F117W} seeds to nucleate their own aggregation as well as that of NM^{wt}. The addition of 5% NM^{wt} seeds accelerated the conversion of soluble NM^{F117W} into amyloid fibrils at the same rate as NM^{F117W} seeds (not shown). Similar results were obtained using NM^{F117W} to seed soluble NM^{wt} protein (not shown), suggesting that the substitution at position 117 does not alter the structural complementarities between NM^{wt} and NM^{F117W}. Taken together, these initial observations suggest that the Phe → Trp substitution at position 117 does not alter the physical properties of the NM domain of Sup35 protein.

Monitoring the Fibrillation Properties of the NM Domain by Trp Fluorescence Emission and Polarization: The Region around Position 117 Assumes Its Final Position Early in Aggregation. The presence of a Trp residue in the NM domain creates a new opportunity to investigate the aggregation properties of this domain *in vitro*. Soluble NM^{F117W} presents a center of spectral mass of Trp emission that is completely red shifted (355 nm), suggesting, as expected, that Trp 117 is extensively exposed to the aqueous environment in the soluble protein (Figure 1A and insert). The insert also shows the expected lack of emission by NM^{wt} when excited at 295 nm. Upon fibril formation (Figure 1A), the center of spectral mass shifts 5 nm toward the blue (350 nm), indicating that the region around Trp 117 moves from its completely exposed position to a lesser exposed region as aggregation proceeds. Although a shift of 5 nm is significant, the value at 350 nm indicates that there is still some solvent accessibility in this region. It should be noted that the spectroscopic properties of Trp 117 do not change when

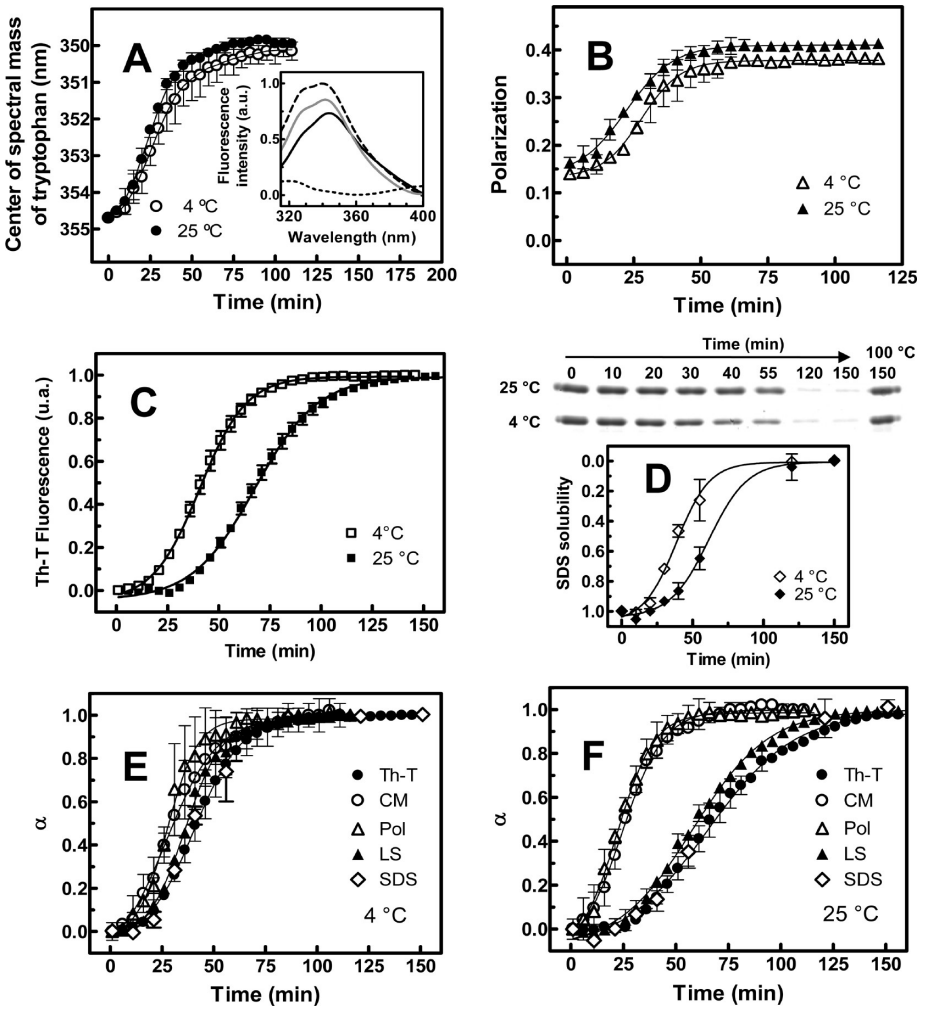

FIGURE 1: Time courses of NM^{wt} and NM^{F117W} aggregation at 4 or 25 °C, as measured by different probes. (A) Changes in the center of spectral mass of Trp 117 during aggregation of NM^{F117W} at 4 °C (open circles) or at 25 °C (filled circles). The insert represents the emission spectra of soluble NM^{F117W} (solid black line) grown at 25 °C (dashed line) or at 4 °C (solid gray line). For comparison, the emission spectrum of NM^{wt}, where no Trp emission was detected (dotted line), is also shown. (B) Changes in fluorescence polarization during the aggregation of NM^{F117W} at 4 °C (open triangles) and at 25 °C (filled triangles). (C) Changes in thio-T binding during the aggregation of NM^{F117W} at 4 °C (open squares) and at 25 °C (filled squares). (D) Changes in SDS solubility during the aggregation of NM^{F117W} at 4 °C (open diamonds) and at 25 °C (filled diamonds). The upper gels show the bands with which the extension of SDS solubility was evaluated. NM^{F117W}-fibril formation at 4 °C (E) or 25 °C (F) was evaluated by thio-T binding (filled circles), the shift in the center of spectral mass of Trp 117 (open circles), polarization (open triangles), light scattering (filled triangles), and SDS solubility (diamonds).

NM^{F117W} is heated to 90 °C (not shown), a condition that causes increased secondary structure but not aggregation (*38*).

Fluorescence polarization measurements are suitable for measuring the formation of molecular assemblies such as protein−DNA complexes, protein oligomers, or, as reported here, fibril formation (Figure 1B) (*39*, *40*). In the soluble state, the polarization value of NM^{F117W} was 0.15; this value increased to 0.4 upon fibril formation (Figure 1B). The polarization value of Trp 117 in the soluble, monomeric state of NM^{F117W} (0.15) is higher than expected, probably due to the contribution of the global rotation of the protein and local motions of Trp 117. Again, there were no significant differences in kinetics of aggregation at 4 or 25 °C; the $t_{1/2}$ values were 27 ± 2 and 22 ± 3 min, respectively (Figure 1B and Table 1).

Interestingly, when Trp fluorescence emission (center of spectral mass) was used as a reporter of fibril formation, there was no difference in the fibrillation rates at 4 and 25 °C (Figure 1A), in contrast to data generated by thio-T binding (Figure 1C). By following Trp fluorescence, the $t_{1/2}$ values observed were 27 ± 3 min at 4 °C and 24 ± 2 min at 25 °C, while by monitoring thio-T revealed $t_{1/2}$ values of 40 ± 3 min at 4 °C and 67 ± 3 min at 25 °C (Table 1). In addition, when SDS resistance was used to report fibril formation, a difference was noted in fibrillation rates at 4 and 25 °C (Figure 1D), and the profiles overlapped with those generated by thio-T binding (Figure 1E,F).

Panels E and F of Figure 1 compare the extent of fibrillation (α) of NM^{F117W} at 4 and 25 °C, respectively, as followed by thio-T binding, a light scattering increase, a shift in the center of mass of Trp emission, SDS resistance, and an increase in polarization. When fibrillation was performed at 25 °C (Figure 1F), the changes in the center of mass of Trp emission and polarization occurred before the changes were observed for thio-T binding, SDS resistance, and light scattering. After 50 min of aggregation at this temperature, almost all of the spectroscopic changes related to Trp 117 had already occurred, while the changes in the fluorescence properties of thio-T and SDS resistance, fibril indicators, had changed only ~20%. Curiously, at 4 °C (Figure 1E), the changes in Trp 117 spectroscopy, thio-T binding, SDS resistance, and light scattering

occurred in an almost concerted fashion, leveling off at around 50−60 min (Table 1).

Taken together, these results suggest that very early in the aggregation process of the NM domain, when the nucleus is formed (nucleation phase), the region around position 117 already assumes its final position, regardless of the temperature employed during fibril formation. Next, the growth of this nucleus into fibrils through the addition of soluble species (extension phase) is temperature-dependent, occurring faster at 4 °C. Thus, the spectroscopic properties of Trp 117 allow us to determine the steps in the aggregation of the NM domain that are temperature-sensitive. The lag phase is temperature-independent, leading to the formation of a species that does not yet bind thio-T but holds the region around position 117 in its final conformation that seems to be slightly solvent accessible (*16*, *41*, *42*). However, the exponential phase depends on the temperature, leading to the formation of mature fibrils that bind thio-T.

To gain additional insight into the accessibility of Trp 117 in the soluble versus aggregated NM domain, acrylamide quenching was performed (*43*). Figure 2 shows the Stern−Volmer plots for the soluble and fibrillar forms of NM^{F117W} grown at 4 or 25 °C, which were used to determine the Stern−Volmer constants (K_{SV}, slopes of the plots). The soluble protein has a K_{SV} of 12.38 ± 0.42 M^{-1}, indicating, as expected, that Trp 117 is solvent-exposed. The K_{SV} for fibrils grown at 25 and 4 °C were much lower: 5.35 ± 0.27 and 7.18 ± 0.18 M^{-1}, respectively, confirming the burial of Trp 117.

Are the Nuclei Elements of Self-Propagating Structural Information or Is This Property Restricted to the Seeds? It has been shown that the addition of seeds obtained by fractionation of a suspension of preformed fibrils can accelerate the fibrillation process of several amyloidogenic proteins, including Sup35 (*11*, *44*). In several cases, these seeds can also transfer structural information to the next generation of growing fibrils (*21*, *41*, *45*) regardless of the experimental conditions in which the daughter fibrils grow. Thus, these seeds catalyze the aggregation reaction and propagate the structural information that was present in the fibrils from which they originated. While these two functions are interrelated, they can be probed separately as shown below.

We wanted to test whether the nucleus that is formed in the lag phase of spontaneous aggregation reactions already has structural information that could be passed to the next generation of growing fibrils. In other words, we asked if the structural information is restricted to seeds, which are small pieces of mature amyloid fibrils, or if information could be inherent to and propagated by the nuclei.

In our first attempt to answer this question, NM^{wt} was incubated under aggregating conditions at 4 or 25 °C for 20 min (time span of the lag phase), and then 5% (w/w) of this suspension was transferred to a solution containing fresh, soluble NM^{wt}. Both the "nucleated" and the control solutions (no added nucleus) were allowed to aggregate in a quiescent condition at 25 °C (Figure 3A) or at 4 °C (Figure 3B). As shown in Figure 3, the addition of a small quantity of nuclei (hollowed symbols) considerably accelerated the aggregation reaction, as detected by Congo Red binding. Since nuclei addition resulted in acceleration that leveled off in less than 10 h, we could not detect any difference between aggregation kinetics at 4 or 25 °C (compare the curves with hollowed circles in panels A and B). This result implies that the nuclei, as expected, are able to act as catalysts of the aggregation reaction even when present at low concentrations.

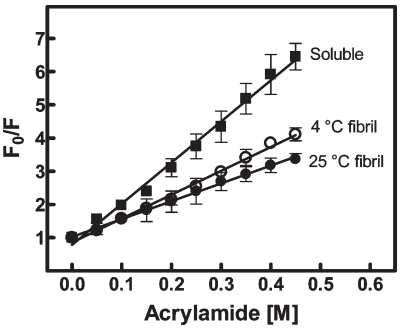

FIGURE 2: Trp 117 is accessible to acrylamide quenching in soluble NM^{F117W} but partially protected in the fibrillar state (Stern−Volmer plots). Small volumes of acrylamide were added to 5 μM soluble (filled squares) or fibrillar NM^{F117W} obtained at 4 °C (hollowed symbols) or at 25 °C (filled circles), and the emission of tryptophan was measured. The initial fluorescence values obtained in the absence of acrylamide were divided by the fluorescence observed after each addition of the quencher (Stern−Volmer plots).

In order to confirm that the fibrils formed in the nucleated samples (hollowed symbols) were constructed from the added nuclei and not from newly formed nuclei, we took advantage of fluorescence correlation spectroscopy (FCS). In FCS measurements, fluctuations arise from the change in the small number of fluorescent molecules that diffuse freely through the excitation volume. The autocorrelation function of the fluctuating signal provides information about the diffusion time of the molecules and the average number of molecules occupying the excitation volume. An increase in particle size, as expected for oligomerization and aggregation processes, is observed as an increase in diffusion times and, consequently, as a shift of the autocorrelation curves to the right (*35*, *46*, *47*).

To perform FCS measurements, the monomeric, soluble NM domain was labeled with FITC, which was used to prepare FITC-labeled nuclei (20 min under aggregating conditions). Five percent of these labeled nuclei was added to a solution of soluble, unlabeled NM domain, which was held for 130 min under quiescent conditions to see whether larger, labeled species would form (fibrils). Figure 3C shows the normalized autocorrelation curves obtained for the FITC-labeled monomeric NM domain (triangles), a solution with FITC-labeled nuclei (circles), and the species obtained from the incubation of 5% FITC-labeled nuclei with 95% unlabeled NM monomers (squares). Labeled NM monomers show a relatively fast diffusion time, with a diffusion coefficient of approximately 90 $\mu m^2/s$ (the coefficient is obtained by fitting the autocorrelation function as described in Experimental Procedures). The autocorrelation function of the FITC-labeled nuclei shifts to longer times compatible with the larger size of these species. Indeed, the average diffusion coefficient calculated for the nuclei was ~0.35 $\mu m^2/s$, confirming their larger size in relation to the NM monomer. Interestingly, the species formed when an aliquot of 5% labeled nuclei was added to a 95% solution of unlabeled monomers exhibited an even larger shift in the autocorrelation function, suggesting that the added FITC-labeled nuclei were used to construct the larger fibrils present. On the other hand, if the labeled nuclei are maintained for the same period of time in the absence of added monomers, no change in particle size is observed and the correlation curve overlaps with that of the labeled nuclei (not shown). These results confirm that the nuclei are included in the larger aggregates formed by recruitment of new monomers in solution.

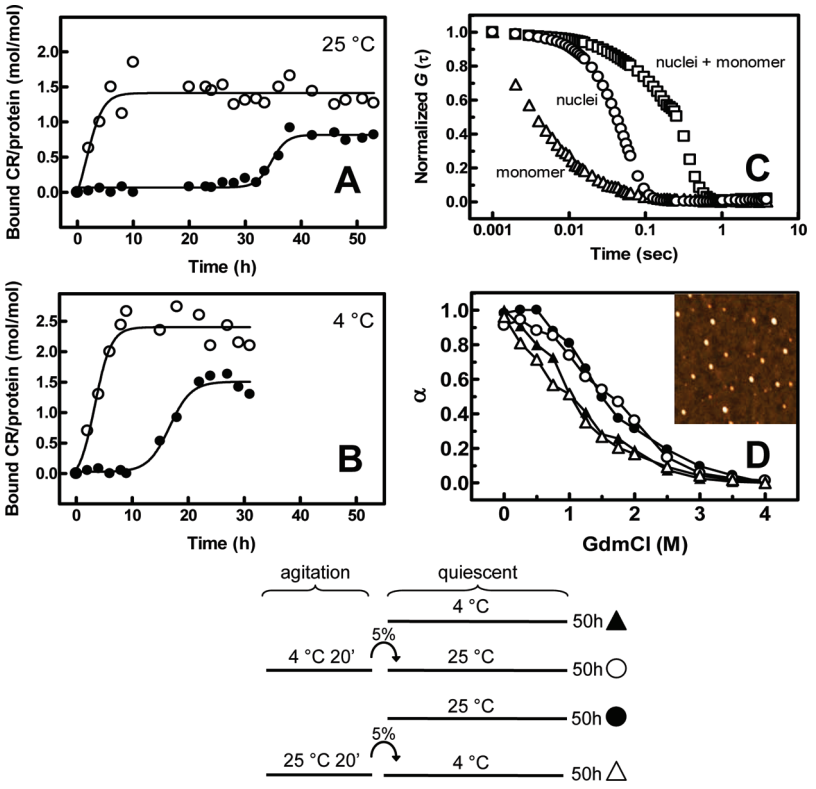

FIGURE 3: Nuclei of NM break the lag phase of NM assembly in quiescent conditions, but they are not able to self-propagate structural information. Soluble NM^{wt} at 5 μM was allowed to aggregate under quiescent conditions in the absence (filled circles) or in the presence of 5% (w/w) nuclei (hollowed circles) at 25 °C (A) or at 4 °C (B). Nuclei formed by stirring 5 μM soluble NM^{wt} at 25 °C or at 4 °C for 20 min were added to samples incubated at 25 and 4 °C, respectively. At the indicated times, the extent of fibril formation was assayed by Congo Red binding. (C) FCS was utilized to obtain autocorrelation curves of 0.25 μM FITC-labeled NM monomers (triangles), 0.25 μM FITC-labeled nuclei (circles), or fibrils formed from a solution containing 5% FITC-labeled nuclei (0.25 μM) incubated for 130 min in the presence of 95% unlabeled NM monomers (4.75 μM) (squares). (D) Soluble NM^{wt} at 5 μM was allowed to aggregate while gently stirring at 4 °C or at 25 °C for 20 min to produce nuclei. Five percent of these nuclei was added to 4.75 μM soluble NM^{wt}, and this suspension was allowed to aggregate for the next 50 h under quiescent conditions at 25 and 4 °C, respectively (see the scheme on the lower position). As a control, two samples were allowed to aggregate at 4 or 25 °C for 50 h under quiescent conditions in the absence of nuclei. After this time, the fibrils were incubated for 2 h with the indicated concentrations of GdmCl (abscissa), and thio-T binding was evaluated. Symbols: (filled triangles) 4 °C/50 h; (filled circles) 25 °C/50 h; (hollowed triangles) 5% nuclei 25 °C → extension at 4 °C/50 h; (hollowed circles) 5% nuclei 4 °C → extension at 25 °C/50 h. The insert shows the AFM image of the species produced after 20 min of aggregation at 4 °C. The image is 2 μm × 2 μm.

Our next approach was to evaluate whether the nuclei, like seeds, could transfer structural information to the next generation of growing fibrils. Fibril stability was probed with GdmCl (Figure 3D), a suitable approach since the fibrils grown at 4 °C are weaker than those grown at 25 °C, allowing us to discriminate between the two sets (see also Figure 5A). The approach that we used was to produce nuclei for 20 min at 4 or 25 °C and then to add 5% of these nuclei to fresh solutions of NM^{wt} (4.75 μM), which were incubated at 25 or 4 °C for 50 h under quiescent conditions (see the scheme at the bottom of Figure 3). As a control, two samples of 5 μM NM^{wt} were allowed to aggregate for 50 h at 4 or 25 °C without agitation. The fibrils were then extracted and incubated in the presence of varying concentrations of GdmCl (mentioned in the abscissa of Figure 3D). Thio-T binding was used as an indicator of fibril integrity.

As seen in Figure 3D, the stability of the fibrils grown at 25 °C, but seeded by nuclei produced at 4 °C, was equal to that observed for the fibrils grown at 25 °C (see the curves with circular data points). The same was true for the inverse experiment in which the nucleation was performed at 25 °C and extension (50 h) was performed at 4 °C (see the curves with triangular data points). The inserts show AFM images of the species that accumulated during the first 20 min of aggregation at 4 °C; only spherical aggregates were seen while no fibrils were detected. Together, these data suggest that structural information present in the fibrils and in the seeds made from them is missing in the nuclei that are formed in the initial steps of the NM aggregation.

In order to gain additional insight into whether the nuclei have inherent structural information for self-propagation, we produced nuclei of different ages (15, 20, and 25 min) at 4 or 25 °C. Then, the temperature of the solution was either maintained (filled symbols in Figure 4) or switched from 4 to 25 °C or vice versa (hollowed symbols in Figure 4). These solutions were incubated with agitation for up to 4 h to complete fibril formation (see the experimental scheme in the upper right position of Figure 4). The fibrils were then withdrawn and incubated in the presence of varying concentrations of GdmCl (mentioned in the abscissa of Figure 4) to check their integrity by thio-T.

As seen in Figure 4A, the stability of the fibrils that were at 4 °C for 15 min before being transferred to 25 °C (4 h extension) was equal to that observed for the fibrils that remained at 25 °C for the entire experiment (see the curves with circular data points). The same was true for the inverse experiment in which the nucleation was performed at 25 °C and extension was performed at 4 °C (see the curves with triangular data points). The inserts show AFM images of the species that accumulated during the first 15 min of aggregation at 4 °C; only spherical aggregates were seen, and no fibrils were detected. Figure 4B

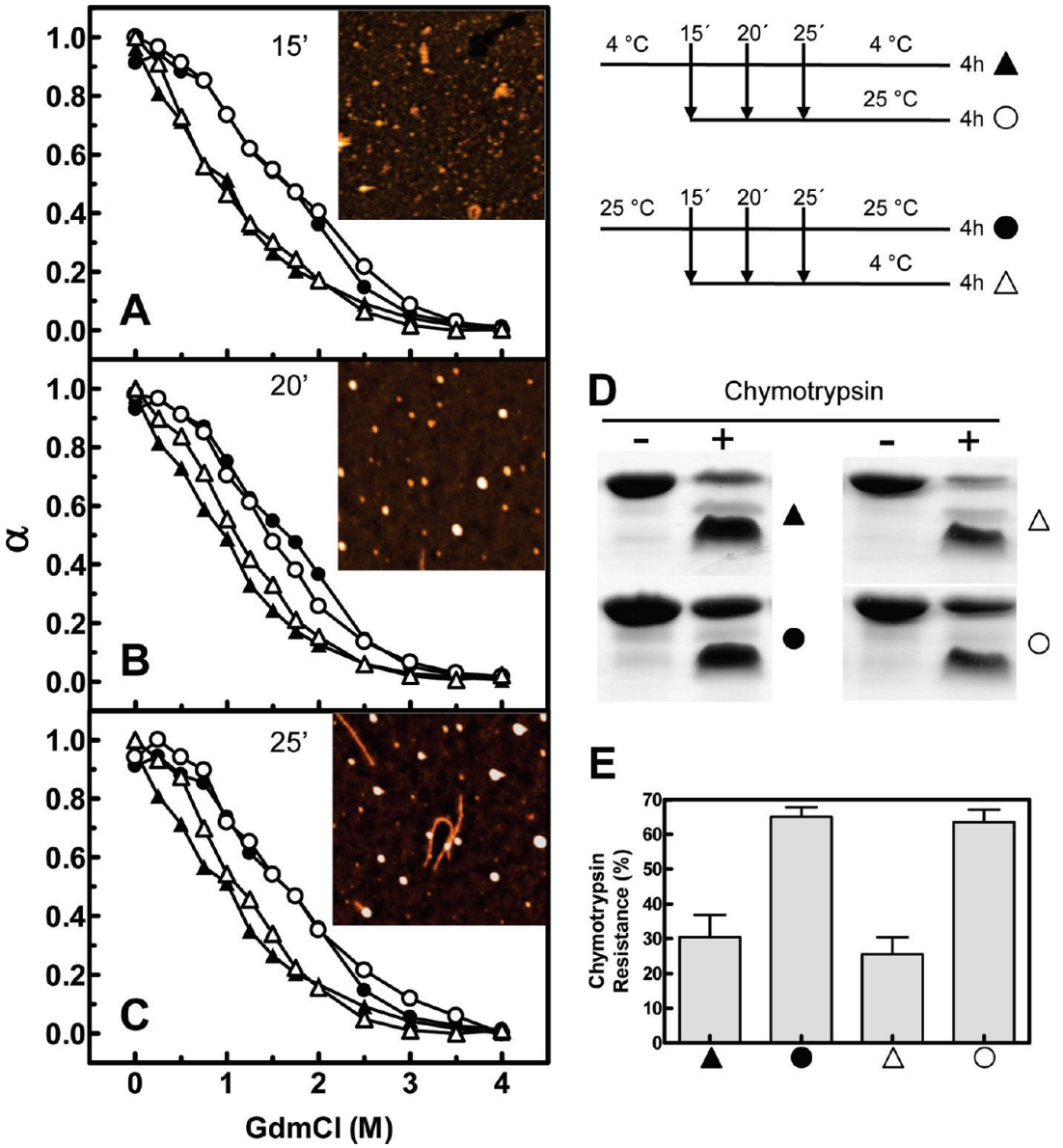

FIGURE 4: Nuclei or small oligomers of the NM do not yet contain the self-perpetuating information that is present in small fibrils or seeds. Soluble NM^{wt} at 5 μM was allowed to aggregate under gentle stirring at 4 °C or at 25 °C for 15 (A), 20 (B), or 25 (C) min; then, the temperatures were switched (4 → 25 °C and 25 → 4 °C) for the next 4 h. As a control, two samples were allowed to aggregate at 4 or 25 °C for 4 h (see scheme on the upper right position). After the allotted time, the fibrils were incubated for 2 h with the indicated concentrations of GdmCl (abscissa), and thio-T binding was evaluated. Symbols in panels A, B, and C: (filled triangles) 4 °C/4 h; (filled circles) 25 °C/4 h; (hollowed triangles) 25 → 4 °C/4 h; (hollowed circles) 4 → 25 °C/4 h. The inserts show the AFM images of the species produced after 15, 20, or 25 min of aggregation at 4 °C. The images of the aggregates formed at 25 °C are not shown due to their similarity to those observed at 4 °C. Each image is 2 μm × 2 μm. (D) Digestion pattern of the fibrils from panel C (same symbols as in panel C). Note that the fibrils grown at 4 °C are more susceptible to chymotrypsin than the 25 °C grown fibrils, and this pattern did not change after the temperature shift (open triangles and circles). (E) Quantification of the gels present in panel D.

presents the data from the experiment in which the nuclei were produced during 20 min at 4 or 25 °C before the temperature switch. A similar result was obtained for this experiment, although a slight difference in stability of these fibrils was observed. AFM images of the aggregates formed during the first 20 min of aggregation at 4 °C show the absence of mature fibrils and the presence of only spherical aggregates (insert in panel B). Even when more mature nuclei were used as seeds (25 min nuclei growth), similar results were obtained (Figure 4C), suggesting again that nuclei are not able to self-propagate their structural information. However, to perform the experiment described in panel C, we had to centrifuge briefly the solution before shifting the temperature due to the presence of small fibrils already formed. As seen in the insert of panel C, only small, reminiscent fibrils were present among a majority of round aggregates in the nuclei suspension.

We confirmed this result by evaluating the chymotrypsin resistance of the fibrils (Figure 4D,E). Fibrils grown at 4 °C for the entire period exhibited a similar resistance against chymotrypsin as those fibrils grown at 4 °C in the presence of nuclei grown for 25 min at 25 °C (see the data presented as triangles). The same was true for the fibrils grown at 25 °C (see the data presented as circles), which indicated an enhanced resistance to chymotrypsin digestion (*21*).

Circular dichroism (CD) was utilized in order to gain insight into the secondary structure content of the nuclei formed during

these times of aggregation (15, 20, and 25 min) at 4 and 25 °C (Supporting Information, Figure S2A,B). We emphasize that the spectra represent the secondary structure content of the whole population of molecules present at the time points of the aggregation reaction, including any unfolded, soluble protein still present in solution, which makes spectra interpretation somewhat tenuous. Nevertheless, early aggregates or nuclei were found to have increasing β-sheet content over the course of maturation while still retaining a random coil structure (minimum close to 200 nm) that is absent from the mature amyloid fibrils. Thus, the small oligomers or nuclei formed at 4 and 25 °C have similar secondary structures, as seen by CD, and tertiary structures, as measured by Trp fluorescence, and they are not yet able to self-propagate structural information.

These data suggest that the self-perpetuating structure of the amyloid fibril of the NM domain seems to be absent from the early aggregates that are formed in the initial steps of NM aggregation. The structure of the nuclei formed at 4 °C seems to be similar to that of the nucleus formed at 25 °C; the differences in morphology described for fibrils grown at these two temperatures must be obtained in later steps of the NM aggregation process. These results are in agreement with Petkova et al. (*48*), who showed that, although quiescent fibrils of Aβ 1−40 are different from the agitated fibrils in several aspects, including toxicity, early aggregates of both types had similar toxicities, indicating a lack of self-perpetuating structural conformation at this stage of aggregation.

Using Trp 117 Fluorescence Emission To Evaluate Fibril Stability: 4 versus 25 °C Grown Fibrils. To study the difference in stability of fibrils grown at 4 or 25 °C, we compared the GdmCl-induced dissociation−denaturation profiles of the NM^{F117W} fibrils (Figure 5A) by measuring a decrease in thio-T binding (circles) and the red shift in the center of mass of Trp emission (triangles). The data are expressed as extent of reaction (α), and the insert shows the raw data of the center of spectral mass.

With thio-T fluorescence, we observed fibril dissociation at lower GdmCl concentrations (circles) than when we assayed with Trp fluorescence (triangles), in which the red shifts were found to vary from 350 to 355 nm (insert). The fibrils grown at 4 °C ($GdmCl_{1/2}$(thio-T) = 0.96 M and $GdmCl_{1/2}$(Trp) = 1.9 M) were less resistant to GdmCl treatment than the fibrils produced at 25 °C ($GdmCl_{1/2}$ for thio-T = 1.7 M and $GdmCl_{1/2}$ for Trp = 2.7 M), a finding that is consistent with the previous observation that fibrils grown at 4 °C are more disordered than those grown at 25 °C (*16*, *21*).

We also investigated the effects of high hydrostatic pressure (HHP) on fibrils of NM^{F117W} grown under different temperatures (Figure 5B,C). HHP is a physical tool to modulate protein−solvent interactions through a volume change caused by elimination of void volumes and hydration of amino acid groups (*49*). HHP was recently applied to evaluate amyloid stability, using transthyretin and α-synuclein as models (*50*). When the fibrils grown at 25 °C (Figure 5B) or 4 °C (Figure 5C) were subjected to HHP in the absence of GdmCl (circles), there was an increase in thio-T binding, in contrast to the decrease that was observed in the dissociation experiment with GdmCl. This result suggests that the amyloid structure is preserved under pressure and, perhaps, assumes a distinct conformation that is able to accommodate more molecules of thio-T. Curiously, the fibrils grown at 4 °C were even more capable of binding thio-T under pressure than fibrils grown at 25 °C, which suggests that their structures

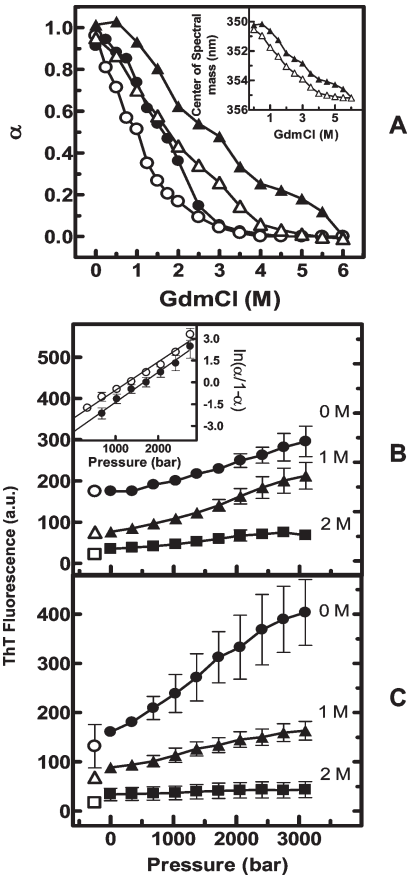

FIGURE 5: GdmCl induces dissociation−denaturation of the NM^{F117W} fibril while high hydrostatic pressure (HHP) induces only a structural modification on fibril architecture. (A) Comparing the stability of the NM^{F117W} 4 and 25 °C grown fibrils against GdmCl induced dissociation−denaturation. Preformed fibrils at 5 μM were incubated with the indicated concentrations of GdmCl (abscissa) for 2 h; then, the center of mass of Trp emission (triangles) and thio-T binding (circles) were evaluated. The data for fibrils grown at 4 °C are represented by hollow symbols while data for 25 °C grown fibrils are demarcated by filled symbols. The insert shows the raw data for the shift in the center of mass of Trp emission for fibrils grown at 25 °C (filled triangles) or 4 °C (open triangle). Fibrils at 5 μM obtained at 25 °C (B) or at 4 °C (C) were subjected to increasing pressure, and the binding of thio-T was measured after a 10 min equilibration. The fibrils were compressed in the absence (circles) or in the presence of 1 (triangles) or 2 M (squares) GdmCl. Note that there is an increase in thio-T binding when pressure is applied, suggesting a rearrangement of fibril structure rather than dissociation. The open symbols at the left represent the return to atmospheric pressure. (Insert) Plot of $\ln(\alpha/(1-\alpha))$ versus pressure for the data presented in panels B and C (absence of GdmCl). The $\Delta G_{F1\rightarrow F2}$ and $\Delta V_{F1\rightarrow F2}$ were obtained from the intercepts and the slopes, respectively. Filled and hollow symbols represent the 25 and 4 °C grown fibrils, respectively.

are indeed different. Light scattering did not change under pressure, reinforcing the conclusion that the fibrils are intact (not shown). Also, the center of spectral mass of Trp 117 was slightly red shifted upon compression by 2 and 1.5 nm for the 4 and 25 °C grown fibrils, respectively (not shown). This slight red shift induced by pressure indicates that Trp 117 is not as exposed in either type of fibrils as it is in the soluble protein.

The ability to bind thio-T under pressure was gradually lost when increasing concentrations of GdmCl were added to the pressure buffer (triangles and squares in Figure 5B,C). This result was expected because the addition of 1−2 M GdmCl was already found to produce some fibril dissociation (Figure 5A). It is important to note that, after returning to atmospheric pressure,

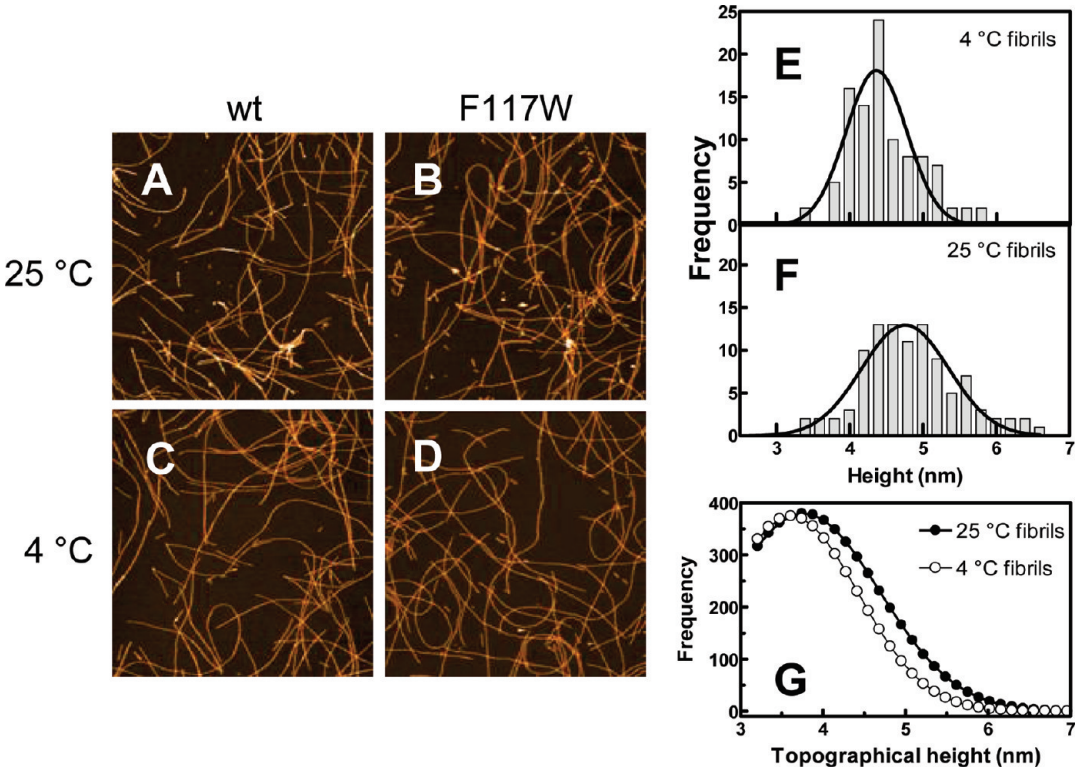

FIGURE 6: The fibrils produced at 25 °C are larger than those grown at 4 °C. AFM images of the fibrils of NM^{wt} (A and C) and NM^{F117W} (B and D) aggregated at 25 °C (A and B) or 4 °C (C and D). Each image is 5 μm × 5 μm. The height frequencies of fibrils of NM^{wt} aggregated at 4 °C (E) or 25 °C (F) are statistically different. (G) Gaussian fit to topographical height distribution of Sup35 fibrils aggregated at 25 °C (closed symbols) or 4 °C (open symbols).

the thio-T binding property was rescued (isolated symbols in the left of panels B and C), suggesting that the structural changes induced by HHP on fibril architecture are reversible. Indeed, AFM images of these "post pressure" fibrils showed no differences in morphology (not shown).

Taken together, these data suggest that the amyloid fibril of the NM domain of Sup35 exists in two different states, which we designate here as F1 and F2. F2 is formed under pressure and has an enhanced thio-T binding capacity. From the data in Figure 5B,C, we calculated the volume and the free energy changes associated with this conversion (F1↔F2) according to eq 3 (Experimental Procedures; insert of Figure 5B). The volume changes in the conversion of F1 → F2 were 51 and 48 mL/mol, while the changes in free energy were 2.03 and 1.47 kcal/mol at 25 and 4 °C, respectively.

AFM Reveals Small but Significant Differences between the Fibrils Grown at 4 or 25 °C. We applied AFM quantitative imaging analyses to the Sup35 fibrils grown at 25 °C (upper images) and 4 °C (lower images). Representative images of surface-absorbed NM^{wt} (left images) and NM^{F117W} (right images) fibrils that were acquired using noncontact AFM are shown in Figure 6A−D. The fibrils composed of NM^{F117W} are indistinguishable from the NM^{wt} fibrils in terms of morphology, regardless of the temperature employed during aggregation.

As previously reported (*16*, *21*), the core of the fibrils of an NM domain that was grown at 4 °C seems to be shorter than the one composed of fibrils that were grown at 25 °C (encompassing residues 31−86 and 21−121, respectively). Thus, the fibril grown at 4 °C possesses an additional extended segment that weakens its structural stability. These conclusions were raised based on the behavior of different fluorescent probes attached to different points in the sequence of the NM domain (*16*). We wondered if it were possible to visualize this slight difference in morphology by AFM, so we examined the height of the cross section of 150 individual fibrils of NM^{wt} grown at 25 or 4 °C. The mean height of the fibrils grown at 25 °C was 4.83 ± 0.58 nm (mean ± standard deviation, n = 150), whereas the mean for fibrils grown at 4 °C was 4.47 ± 0.45 nm (mean ± standard deviation, n = 150). This difference, while very small, is significant ($P < 0.001$ in Tukey's test, Experimental Procedures). There are also consistent differences in the Gaussian histograms of height distributions for the fibrils grown at both temperatures (Figure 6E,F). While the Gaussian distribution of 4 °C grown fibrils is centered about 4.36 ± 0.41 nm, the height distribution for the 25 °C grown fibrils is centered about 4.75 ± 0.59 nm. We also measured the topographical height, which allows the analysis of the whole image rather than individual fibrils (*51*). Using this analysis, we quantified the height frequency above a threshold of 3 nm. Figure 6G shows the consistent differences that we observed in the Gaussian fits of the 25 and 4 °C fibrils after considering 66000 points per sample.

DISCUSSION

We constructed an NM mutant of the Sup35 protein that contained a tryptophan residue at position 117, which we used to probe the aggregation process of this protein. This approach takes advantage of the sensitivity of Trp to its surrounding environment, which can be monitored by changes in spectroscopic behavior. Interestingly, this probe allowed us to more thoroughly dissect the mechanism of aggregation and examine the effect of temperature (4 and 25 °C) on the kinetics of NM-fibril formation.

The fibrillation process of the NM domain can be divided simplistically into two steps: a lag phase, in which part of the soluble protein oligomerizes and transitions into an amyloidogenic nucleus (small oligomer), and an assembly phase (extension), in which the remaining soluble protein rapidly associates with this nucleus and becomes an amyloid fibril (*14*−*16*). The data presented here suggest that temperature does not affect the first step of NM fibrillation, which is better visualized by analyzing the changes in the spectroscopic behavior of the Trp residue introduced at position 117. At 4 or 25 °C, the shift in the center of mass of Trp 117, as well as the increase in polarization, occurred with identical kinetics. However, the second step of NM fibrillation, which is better visualized by an increase in light scattering, SDS resistance, and thio-T binding, is affected by temperature, occurring faster at 4 °C (Figure 1 and see the slopes of each curve in parentheses in Table 1).

Previous studies have already addressed this curious effect of low temperature on the kinetics of *in vitro* NM aggregation (*14*, *52*) and the strength of the [PSI^+] phenotype (*21*). Serio and collaborators (*14*) were the first to show that aggregation of the NM domain of Sup35 is faster at low temperatures, a counterintuitive observation given that, in general, low temperatures inhibit fibril formation. Scheibel and Lindquist explained this observation with the idea that agents that diminish NM flexibility also diminish NM aggregation, e.g., high temperature, osmolytes, and the deletion of the repeats in the NM domain (*38*).

In an elegant study performed by Krishnan and Lindquist (*16*), the analysis of the solvent accessibility of 37 cysteines introduced throughout the sequence of the NM domain and the behavior of attached fluorescent probes were used to construct a structural model for a fibril grown at 25 °C. Although a model for these fibrils was not presented in this study, by using the same approach, it was possible to detect a structural distinction between these two types of fibrils. It has been postulated that fibrils grown at 4 °C have a shorter core, made up of residues 31−86, than the central core of the fibrils grown at 25 °C, which spans residues 21−121. Data from our acrylamide quenching experiments are also consistent with this observation since the Stern−Volmer constants obtained indicate that Trp 117 is slightly more solvent exposed in the fibrils grown at 4 °C than in those grown at 25 °C. Also, through the use of excimer formation (*16*), it was possible to map the intersubunit interface, which turned out to be shorter in the 4 °C grown fibrils. Taken together, these observations provide an explanation for why the fibrils grown at 4 °C are more easily fractured than those grown at 25 °C. The fragility of these fibrils would also explain why they produce a stronger phenotype when introduced in yeast cells (*21*) since mother cells pass pieces of prions to their daughters, which more easily perpetuate the cycle of conversion.

In Linquist's study (*16*), the cysteines at positions 112 and 121 are closest to Trp 117. Interestingly, these probes produced conflicting data. Positions 112 and 121 were partially accessible to pyrene maleimide in the fibrils grown at 25 °C after 3 h of labeling, whereas experiments performed with an acrylodan label suggested that these positions were sequestered from the solvent after NM fibrillation. The authors suggested that this region of the fibril may be fluctuating between an extended and folded conformation. Our data are consistent with the data presented by Krishnan and Lindquist (*16*), and we suggest that residues 112, 117, and 121 are located at the border between the core domain and the extended segment of the fibril. This conclusion is based on the data from the partial blue shift of Trp emission upon aggregation as well as data from acrylamide quenching (Figures 1 and 2). Recently, Toyama et al. (*42*) used hydrogen−deuterium exchange coupled with solution NMR spectroscopy to dissect the structural differences in the fibrils of the NM domain grown at 4 and 37 °C. They showed that the core of the fibrils grown at 37 °C spans the first 70 residues, while the core of the fibrils formed at 4 °C is shorter, including only the first 40 residues. Again, position 117 in both fibrils seems to be in a position of the amyloid fibril that is not completely exposed nor completely protected.

Krishnan and Lindquist (*16*) proposed in their study that the establishment of the head-to-head contacts is responsible for the lag phase in NM aggregation. In their model, the head region comprised the first 40 amino acids of the NM domain; the labeled cysteines inserted into this region completed all spectroscopic changes without a lag phase in less than ~50 min. In our study, however, we note that the Trp inserted at position 117, though far from the head region of the NM domain, also completed all changes in its spectroscopy in less than 50 min in a temperature-independent fashion with a very short lag phase (Figure 1). We suggest that the segment around this position accompanies the structural modification that is necessary for the formation of head-to-head contacts and a nucleus. Indeed, in this study it was also suggested that the region of the M domain close to the N domain (region around position 117) becomes structured only when N residues convert to amyloid while the distal region of the M domain remains unstructured after fibril formation. Thus, we postulate that the 5 nm shift observed in Trp 117 emission during the early steps of NM aggregation reflects a structural modification that takes place in the proximal region of the M domain, which seems to become structured upon N organization.

Additionally, our data indicate that the structural modification that leads to the formation of this early collapsed aggregate is not influenced by temperature (nucleation event). The extension reaction (conversion of the nuclei/small oligomers into mature fibril) seems to be an enthalpy-driven process that is favored by lower temperature. During extension, temperature shapes the final structure of the amyloid fibril; i.e., the fibril is loosely packed at 4 °C and more compact at 25 °C (Figures 5 and 6). Our data suggest that the nuclei or small aggregates do not have the self-propagation feature (Figures 3D and 4) that is presented by the fibrils or by the seeds (pieces of fibrils) although, as shown by FCS measurements (Figure 3C), they are incorporated in the fibril. Nevertheless, Orte and collaborators (*53*) recently showed by single-molecule fluorescence a myriad of highly heterogeneous oligomers of the SH3 domain, whose stability increases with time before incorporation into amyloid fibrils. Thus, it is possible that there is a specific population of mature oligomers that are able to self-perpetuate structural information onto growing fibrils. In the case of Sup35, since the lag phase was very short under the experimental conditions utilized here, the isolation of such a specific population of oligomers would be very difficult.

There is still no definitive model of the Sup35 fibril. Several studies have found Sup35 to form a β-helical structure with head-to-head and tail-to-tail interactions in which the tail region length determines differences in fibrils and, consequently, phenotypes of the strain (*21*, *22*). More recently, Tycko's group (*18*, *19*) used solid-state NMR on Sup35 fibrils to show an in-register parallel β-sheet structure in which some regions of the M domain become structured in the amyloid fold. They suggest that structural variations in the M domain may be responsible for the differences in prion strains. If this model is indeed correct, it is possible that

at the nucleus stage the in-register parallel β-sheet structure is still not completely defined and not influenced by the temperature at which nuclei form, as suggested here.

Here, we also evaluated the stability of Sup35 fibrils grown at 4 or 25 °C against dissociation−denaturation by GdmCl (Figure 5A) and HHP (Figure 5B,C). As previously shown, the fibrils grown at low temperature are less stable than the ones grown at a higher temperature (*16*, *21*). By using NM^{F117W}, we were able to separate the dissociation and denaturation processes, with the former occurring in lower GdmCl concentrations.

HHP causes dissociation and denaturation of proteins due to the existence of a void volume in the protein native state (*54*). The effects of HHP on amyloid fibrils vary according to the protein of interest, experimental conditions, and age of the aggregates (*50*, *55*). In the case of NM amyloid fibrils, instead of disrupting the fibrils, HHP induces a new structural organization that is able to accommodate more thio-T molecules, similar to what has been reported for β2-microglobulin (*56*). Rearrangements of the amyloid fibril into a new conformation have been observed with prion protein (PrP) after heat treatment in the presence of Triton X-100 (*57*). Interestingly, the fibrils grown at 4 °C were able to incorporate more thio-T under pressure than the fibrils grown at 25 °C (Figure 5B,C); this result could be explained by the greater compactness of the latter. The structural changes caused by HHP in the absence of GdmCl were reversible, which allowed us to obtain the thermodynamic parameters associated with this structural transition (Figure 5). From the estimated changes in volume ($\Delta V = 48.31 \pm 1.83$ mL/mol and $\Delta V = 51.09 \pm 3.39$ mL/mol for the 4 and 25 °C fibrils, respectively), we observed that both fibrils are converted into a more packed state that occupies lower volumes. The volume change recorded for β2-microglobulin under pressure was 66 mL/mol (*56*), a value quite similar to the one described here.

The free energy change associated with this transition is low, being even smaller for the fibrils grown at 4 °C ($\Delta G = 1.47 \pm 0.07$ kcal/mol and 2.03 ± 0.15 kcal/mol for the 4 and 25 °C grown fibrils, respectively). Pressure mainly interferes with hydrophobic and ionic interactions and eliminates water-excluded cavities. Hydrogen bonds are insensitive to HHP (*54*). Recently, Nelson and co-workers (*17*) solved the structure of an amyloid fibril composed of a heptapeptide (GNNQQNY) derived from the Sup35 protein. The structure revealed a dry interface between the two sheets and networks of hydrogen bonds among amide groups of glutamine and asparagine side chains. Considering that this pattern of interaction prevails along the amyloid fibril of the entire NM domain, it might explain the insensitivity of NM fibrils to HHP. Upon compression, water infiltrates the interior of the protein and carries more thio-T molecules to the fibril core.

Atomic force microscopy (AFM) has been used extensively to study the morphology and substructure of fibrillar aggregates (*58*). With AFM, several groups have characterized the structural polymorphism of different species of amyloid fibrils (*45*, *59*, *60*). On the basis of these previous observations, we employed AFM to attempt to find morphological differences between the 4 and 25 °C grown fibrils of the NM domain. Indeed, AFM revealed slight but consistent and statistically significant differences between these two types of fibrils (Figure 6). The height of 25 °C grown fibrils was 8% greater than that that of the 4 °C grown fibrils, which is consistent with the existence of a shorter core in the fibril grown at 4 °C (*16*, *21*, *41*, *42*). Moreover, there were differences up to 24% in measurements of mass per length (mpl) of Sup35 amyloid fibrils of distinct classes (*61*), suggesting that Sup35 is able to form polymorphic fibrils that are distinct in shape, degree of polarity, growth rate (*62*), mass per length (*61*), and height (Figure 6). The differences in fibril morphology reported for Sup35 fibrils as well as for other amyloidogenic proteins (*63*, *64*) are probably due to plasticity in the amyloid fold, which is considered an ancient fold (*65*), and must be able to accommodate different primary sequences or similar sequences grown under different conditions in the same archetypal structure.

ACKNOWLEDGMENT

We are grateful to Emerson R. Gonçalves for competent technical assistance and Martha M. Sorenson for a critical reading of the manuscript.

SUPPORTING INFORMATION AVAILABLE

Figure S1 showing that the Phe → Trp substitution at position 117 does not alter the properties of the NM domain of Sup35 protein and Figure S2 depicting the circular dichroism spectra of the species formed during the initial phase (nucleation) of NM^{wt} aggregation at 25 or 4 °C. This material is available free of charge via the Internet at http://pubs.acs.org.

REFERENCES

1. Cohen, F. E., and Kelly, J. W. (2003) Therapeutic approaches to protein-misfolding diseases. *Nature 426*, 905–909.
2. Chien, P., Weissman, J. S., and DePace, A. H. (2004) Emerging principles of conformation-based prion inheritance. *Annu. Rev. Biochem. 73*, 617–656.
3. Wickner, R. B. (1994) [URE3] as an altered Ure2 protein—evidence for a prion analog in *Saccharomyces cerevisiae*. *Science 264*, 566–569.
4. Uptain, S. M., and Lindquist, S. (2002) Prions as protein-based genetic elements. *Annu. Rev. Microbiol. 56*, 703–741.
5. Du, Z., Park, K. W., Yu, H., Fan, Q., and Li, L. (2008) Newly identified prion linked to the chromatin-remodeling factor Swi1 in *Saccharomyces cerevisiae*. *Nat. Genet. 40*, 460–465.
6. Nemecek, J., Nakayashiki, T., and Wickner, R. B. (2009) A prion of yeast metacaspase homolog (Mca1p) detected by a genetic screen. *Proc. Natl. Acad. Sci. U.S.A. 106*, 1892–1896.
7. Patel, B. K., Gavin-Smyth, J., and Liebman, S. W. (2009) The yeast global transcriptional co-repressor protein Cyc8 can propagate as a prion. *Nat. Cell Biol. 11*, 344–349.
8. Alberti, S., Halfmann, R., King, O., Kapila, A., and Lindquist, S. (2009) A systematic survey identifies prions and illuminates sequence features of prionogenic proteins. *Cell 137*, 146–158.
9. Cox, B. S. (1965) A cytoplasmic suppressor of super-suppressor in yeast. *Heredity 20*, 505–521.
10. Derkatch, I. L., Chernoff, Y. O., Kushnirov, V. V., IngeVechtomov, S. G., and Liebman, S. W. (1996) Genesis and variability of [PSI] prion factors in *Saccharomyces cerevisiae*. *Genetics 144*, 1375–1386.
11. Glover, J. R., Kowal, A. S., Schirmer, E. C., Patino, M. M., Liu, J. J., and Lindquist, S. (1997) Self-seeded fibers formed by Sup35, the protein determinant of $[PSI^+]$, a heritable prion-like factor of *S. cerevisiae*. *Cell 89*, 811–819.
12. Perrett, S., and Jones, G. W. (2008) Insights into the mechanism of prion propagation. *Curr. Opin. Struct. Biol. 18*, 52–59.
13. Paushkin, S. V., Kushnirov, V. V., Smirnov, V. N., and TerAvanesyan, M. D. (1997) *In vitro* propagation of the prion-like state of yeast Sup35 protein. *Science 277*, 381–383.
14. Serio, T. R., Cashikar, A. G., Kowal, A. S., Sawicki, G. J., Moslehi, J. J., Serpell, L., Arnsdorf, M. F., and Lindquist, S. L. (2000) Nucleated conformational conversion and the replication of conformational information by a prion determinant. *Science 289*, 1317–1321.
15. Shorter, J., and Lindquist, S. (2005) Prions as adaptive conduits of memory and inheritance. *Nat. Rev. Genet. 6*, 435–450.
16. Krishnan, R., and Lindquist, S. L. (2005) Structural insights into a yeast prion illuminate nucleation and strain diversity. *Nature 435*, 765–772.
17. Nelson, R., Sawaya, M. R., Balbirnie, M., Madsen, A. O., Riekel, C., Grothe, R., and Eisenberg, D. (2005) Structure of the cross-beta spine of amyloid-like fibrils. *Nature 435*, 773–778.

18. Shewmaker, F., Wickner, R. B., and Tycko, R. (2006) Amyloid of the prion domain of Sup35p has an in-register parallel beta-sheet structure. *Proc. Natl. Acad. Sci. U.S.A. 103*, 19754–19759.
19. Shewmaker, F., Kryndushkin, D., Chen, B., Tycko, R., and Wickner, R. B. (2009) Two prion variants of Sup35p have in-register parallel β-sheet structures, independent of hydration, *Biochemistry* (DOI 10.1021/bi900345q).
20. King, C. Y., and Diaz-Avalos, R. (2004) Protein-only transmission of three yeast prion strains. *Nature 428*, 319–323.
21. Tanaka, M., Chien, P., Naber, N., Cooke, R., and Weissman, J. S. (2004) Conformational variations in an infectious protein determine prion strain differences. *Nature 428*, 323–328.
22. Tanaka, M., Collins, S. R., Toyama, B. H., and Weissman, J. S. (2006) The physical basis of how prion conformations determine strain phenotypes. *Nature 442*, 585–589.
23. Royer, C. A. (2006) Probing protein folding and conformational transitions with fluorescence. *Chem. Rev. 106*, 1769–1784.
24. Lakowicz, J. R. (1999) Principles of fluorescence spectroscopy , 2nd ed., Kluwer Academic/Plenum Publishers, New York.
25. Garzon-Rodriguez, W., Vega, A., Sepulveda-Becerra, M., Milton, S., Johnson, D. A., Yatsimirsky, A. K., and Glabe, C. G. (2000) A conformation change in the carboxyl terminus of Alzheimer's A beta (1−40) accompanies the transition from dimer to fibril as revealed by fluorescence quenching analysis. *J. Biol. Chem. 275*, 22645–22649.
26. Li, L., von Bergen, M., Mandelkow, E. M., and Mandelkow, E. (2002) Structure, stability, and aggregation of paired helical filaments from tau protein and FTDP-17 mutants probed by tryptophan scanning mutagenesis. *J. Biol. Chem. 277*, 41390–41400.
27. Dusa, A., Kaylor, J., Edridge, S., Bodner, N., Hong, D. P., and Fink, A. L. (2006) Characterization of oligomers during alpha-synuclein aggregation using intrinsic tryptophan fluorescence. *Biochemistry 45*, 2752–2760.
28. Sambrook, J., Fritsch, E. E., and Maniatis, T. (1989) Molecular Cloning: A Laboratory Manual , 2nd ed., Cold Spring Harbor Laboratory, Cold Spring Harbor, NY.
29. DePace, A. H., Santoso, A., Hillner, P., and Weissman, J. S. (1998) A critical role for amino-terminal glutamine/asparagine repeats in the formation and propagation of a yeast prion. *Cell 93*, 1241–1252.
30. Chien, P., and Weissman, J. S. (2001) Conformational diversity in a yeast prion dictates its seeding specificity. *Nature 410*, 223–227.
31. Gietz, R. D., and Woods, R. A. (2002) Transformation of yeast by lithium acetate/single-stranded carrier DNA/polyethylene glycol method. *Methods Enzymol. 350*, 87–96.
32. Chernoff, Y. O., Uptain, S. M., and Lindquist, S. L. (2002) Analysis of prion factors in yeast. *Methods Enzymol. 351*, 499–538.
33. Paladini, A. A., and Weber, G. (1981) Pressure-induced reversible dissociation of enolase. *Biochemistry 20*, 2587–2593.
34. Kitamura, Y., and Itoh, T. (1987) Reaction volume of protonic ionization for buffering agents—prediction of pressure-dependence of pH and pOH. *J. Solution Chem. 16*, 715–725.
35. Thompson, N. L. (1991) Topics in Fluorescence Spectroscopy (Lakowicz, J. R., Ed.) Vol. 1, p 337, Plenum Press, New York.
36. Muller, J. D., Chen, Y., and Gratton, E. (2003) Fluorescence correlation spectroscopy. *Methods Enzymol. 361*, 69–92.
37. Ludbrook, J. (1998) Multiple comparison procedures updated. *Clin. Exp. Pharmacol. Physiol. 25*, 1032–1037.
38. Scheibel, T., and Lindquist, S. L. (2001) The role of conformational flexibility in prion propagation and maintenance for Sup35p. *Nat. Struct. Biol. 8*, 958–962.
39. Weber, G. (1952) Polarization of the fluorescence of macromolecules. 1. Theory and experimental method. *Biochem. J. 51*, 145–155.
40. Weber, G. (1952) Polarization of the fluorescence of macromolecules. 2. Fluorescent conjugates of ovalbumin and bovine serum albumin. *Biochem. J. 51*, 155–168.
41. Tanaka, M., Chien, P., Yonekura, K., and Weissman, J. S. (2005) Mechanism of cross-species prion transmission: An infectious conformation compatible with two highly divergent yeast prion proteins. *Cell 121*, 49–62.
42. Toyama, B. H., Kelly, M. J. S., Gross, J. D., and Weissman, J. S. (2007) The structural basis of yeast prion strain variants. *Nature 449*, 233–238.
43. Eftink, M. R., and Ghiron, C. A. (1981) Fluorescence quenching studies with proteins. *Anal. Biochem 114*, 199–227.
44. Harper, J. D., and Lansbury, P. T. (1997) Models of amyloid seeding in Alzheimer's disease and scrapie: Mechanistic truths and physiological consequences of the time-dependent solubility of amyloid proteins. *Annu. Rev. Biochem. 66*, 385–407.
45. Jones, E. M., and Surewicz, W. K. (2005) Fibril conformation as the basis of species- and strain-dependent seeding specificity of mammalian prion amyloids. *Cell 121*, 63–72.
46. Eigen, M., and Rigler, R. (1994) Sorting single molecules: application to diagnostics and evolutionary biotechnology. *Proc. Natl. Acad. Sci. U.S.A. 91*, 5740–5747.
47. Schwille, P., Bieschke, J., and Oehlenschläger, F. (1997) Kinetic investigations by fluorescence correlation spectroscopy: the analytical and diagnostic potential of diffusion studies. *Biophys. Chem. 66*, 211–228.
48. Petkova, A. T., Leapman, R. D., Guo, Z. H., Yau, W. M., and Tycko, R. (2005) Self-propagating, molecular-level polymorphism in Alzheimer's beta-amyloid fibrils. *Science 307*, 262–265.
49. Foguel, D., and Silva, J. L. (2004) New insights into the mechanisms of protein misfolding and aggregation in amyloidogenic diseases derived from pressure studies. *Biochemistry 43*, 11361–11370.
50. Foguel., D., Suarez, M. C., Ferrao-Gonzales, A. D., Porto, T. C. R., Palmieri, L., Einsiedler, C. M., Andrade, L. R., Lashuel, H. A., Lansbury, P. T., Kelly, J. W., and Silva, J. L. (2003) Dissociation of amyloid fibrils of alpha-synuclein and transthyretin by pressure reveals their reversible nature and the formation of water-excluded. *Proc. Natl. Acad. Sci. U.S.A. 100*, 9831–9836.
51. Karsai, A., Martonfalvi, Z., Nagy, A., Grama, L., Penke, B., and Kellermayer, M. S. Z. (2006) Mechanical manipulation of Alzheimer's amyloid beta 1−42 fibrils. *J. Struct. Biol. 155*, 316–326.
52. Chien, P., DePace, A. H., Collins, S. R., and Weissman, J. S. (2003) Generation of prion transmission barriers by mutational control of amyloid conformations. *Nature 424*, 948–951.
53. Orte, A., Birkett, N. R., Clarke, R. W., Devlin, G. L., Dobson, C. M., and Klenerman, D. (2008) Direct characterization of amyloidogenic oligomers by single-molecule fluorescence. *Proc. Natl. Acad. Sci. U.S.A. 105*, 14424–14429.
54. Silva, J. L., Foguel, D., and Royer, C. A. (2001) Pressure provides new insights into protein folding, dynamics and structure. *Trends Biochem. Sci. 26*, 612–618.
55. Meersman, F., and Dobson, C. M. (2006) Probing the pressure-temperature stability of amyloid fibrils provides new insights into their molecular properties. *Biochim. Biophys. Acta 1764*, 452–460.
56. Chatani, E., Kato, M., Kawai, T., Naiki, H., and Goto, Y. (2005) Main-chain dominated amyloid structures demonstrated by the effect of high pressure. *J. Mol. Biol. 352*, 941–951.
57. Bocharova, O. V., Makarava, N., Breydo, L., Anderson, M., Salnikov, V. V., and Baskakov, I. V. (2006) Annealing prion protein amyloid fibrils at high temperature results in extension of a proteinase K-resistant core. *J. Biol. Chem. 281*, 2373–2379.
58. Gosal, W. S., Myers, S. L., Radford, S. E., and Thomson, N. H. (2006) Amyloid under the atomic force microscope. *Protein Pept. Lett. 13*, 261–270.
59. Goldsbury, C., Frey, P., Olivieri, V., Aebi, U., and Muller, S. A. (2005) Multiple assembly pathways underlie amyloid-beta fibril polymorphisms. *J. Mol. Biol. 352*, 282–298.
60. Anderson, M., Bocharova, O. V., Makarava, N., Breydo, L., Salnikov, V. V., and Baskakov, I. V. (2006) Polymorphism and ultrastructural organization of prion protein amyloid fibrils: An insight from high resolution atomic force microscopy. *J. Mol. Biol. 358*, 580–596.
61. Diaz-Avalos, R., King, C. Y., Wall, J., Simon, M., and Caspar, D. L. D. (2005) Strain-specific morphologies of yeast prion amyloid fibrils. *Proc. Natl. Acad. Sci. U.S.A. 102*, 10165–10170.
62. DePace, A. H., and Weissman, J. S. (2002) Origins and kinetic consequences of diversity in Sup35 yeast prion fibers. *Nat. Struct. Biol. 9*, 389–396.
63. Nelson, R., and Eisenberg, D. (2006) Recent atomic models of amyloid fibril structure. *Curr. Opin. Struct. Biol. 16*, 260–265.
64. Hess, S., Lindquist, S. L., and Scheibel, T. (2007) Alternative assembly pathways of the amyloidogenic yeast prion determinant Sup35-NM. *EMBO Rep. 8*, 1196–1201.
65. Dobson, C. M. (2003) Protein folding and misfolding. *Nature 426*, 884–890.